



An Empirical Model for Optimizing the Sound Absorption of Single Layer MPP Based on Response Surface Methodology

Al-Ameri Esraa¹, Azma Putra^{2*}, Ali I. Mosa³, R.M. Dan², Osam H. Attia⁴

¹Fakulti Kejuruteraan Mekanikal, Universiti Teknikal Malaysia Melaka, Hang Tuah Jaya, 76100 Durian Tunggal, Melaka, Malaysia

²Centre for Advanced Research on Energy, Universiti Teknikal Malaysia Melaka, Hang Tuah Jaya, 76100 Durian Tunggal, Melaka, Malaysia

³Department of Mechanical Engineering, Collage of Engineering, University of Baghdad, Jadriyah - Baghdad, Iraq

⁴Department of Reconstruction and Projects, University of Baghdad, Jadriyah - Baghdad, Iraq

Abstract. Micro-perforated panel (MPP) is a thin panel absorber capable of absorbing sound energy at a targeted frequency range by adjusting the MPP parameters. An analytical model is available, but it is not a direct, convenient method for practitioners to determine the required MPP parameters. This paper presents an optimized empirical model to calculate the sound absorption coefficient of a single-layer MPP. The response surface methodology is employed for a simple case to generate a second-order polynomial model through a sequence of designing processes to analyze the functional relationships and variation of the outcome performance (sound absorption coefficient) concerning the MPP parameters, namely the panel thickness, hole diameter, perforation ratio, and the depth of the back air layer. The analysis is carried out for frequencies between 300 to 900 Hz. The predicted data (empirical) is compared with the actual data (analytical), leading to a coefficient of variation of 0.145%. The proposed empirical model can be used as a method to select the suitable MPP parameters according to the targeted frequency bandwidth of absorption with less computational time.

Keywords: Optimisation; Response Surface Methodology (RSM); Single layer MPP; Sound absorption

1. Introduction

The Microperforated panel (MPP) absorber proposed by Maa (1975) has been widely used as a next-generation sound absorbers system (Mosa et al., 2018). It has the advantages of providing a high sound absorption coefficient, ease of installation, fine washability, environmental friendliness, and attractive appearance (Tayong et al., 2018; Yang et al., 2019), as an alternative to porous absorbing materials (Ahmad & Salih, 2020; Prasetyo et al., 2020). Aimed for a wide absorption bandwidth; many studies have been presented on a single layer MPP using various techniques. This includes the presents of the MPP model with incompletely partitioned cavities (Huang et al., 2017) broadband MPP model with ultra-MPP (Qian et al., 2014a); thin MPP models (Prasetyo et al., 2021), inhomogeneous MPP systems with multiple cavity depths (Prasetyo et al., 2016; Mosa et al., 2019; Kusaka

*Corresponding author's email: azma.putra@utem.edu.my, Tel.: +606-2704341; Fax: +606-2701046
doi: [10.14716/ijtech.v13i3.5507](https://doi.org/10.14716/ijtech.v13i3.5507)

et al., 2021).

The analysis and optimization of the MPP parameters to enhance the absorption performance have been presented (Qian et al., 2014b; Yu et al., 2016); however, most of these processes are consumed time with convoluted processing steps, especially models of a large structure (Hussein, 2020; El-Basheer et al., 2017). Generally, it should be considered that the potential interactions between model variables could cause incorrect optimum parameters as any modifying parameter at a time. In order to minimize these computational efforts, the approach of the response surface methodology (RSM) has been employed to implement the optimization of the acoustic absorption for numerous noise control applications (Liang et al., 2007; Harahap et al., 2019; Wang et al., 2017; Wahab et al., 2019).

Box and Wilson (1951) first presented this method to initialize and evolve empirical models and by providing the basic principles framework of RSM, they denote the response process. Randall P. and Terence J. (Niedz & Evens, 2016) attained a review discussing the theoretical aspects and practical applications of RSM literature. Essentially, the RSM involves replacing the complete procedure along with an empirical model by collecting a series of results at several detached points within the design domain. The impression of the second-order functions is because of the low-order processes are powerful, since generating the corresponding response surface is fast and cheap. (Boulandet & Lissek, 2010; Hawashi et al., 2019; Petrus et al., 2021; Saleh et al., 2021).

Even though several studies have been presented on the absorption performance of MPP using analytical or simulation methods. Still, they are not direct, convenient methods for practitioners to determine the required MPP parameters. Thus, the current study uses a factorial design of experiment software to present a novel empirical model for a single-layer-MPP absorber based on RSM to contribute a straightforward and more accessible model with less computational time. Furthermore, to optimize the relationship between the model parameters (holes diameters and ratio, cavity depth, and panel thickness). The paper structure presents recent studies on the MPP and the RSM, followed by the empirical model theories and generation methodology step. Section 3 summarized the model validation and predicted results. The conclusion of the study is present at the end.

2. Methodology

2.1. Maa model

The basic theory of the traditional single-layer MPP absorber model has been presented by Maa (1975; 1987). Usually, the MPP comprises holes of a similar size and uniformly distributed over the panel surface. The mathematical model of the acoustic impedances using the electrical equivalent circuit method can be expressed as the following Equations:

$$Z_{MPP} = Z_{\text{resistance}} + Z_{\text{reactance}} \quad (1)$$

$$Z_{MPP} = \frac{32\eta t}{\rho c p^2} \left(\sqrt{1 + \frac{x^2}{32}} + \frac{xd\sqrt{2}}{8t} \right) + \frac{t}{\rho c} \left[1 + \left(9 + \frac{x^2}{2} \right)^{-1/2} + \frac{0.85d}{t} \right] \quad (2)$$

Where Z_{MPP} in Equations 1 and 2 represents the panel impedance, then the total acoustic impedance and the sound absorption coefficient of the system including the impedance of the air cavity can be expressed as in Equations 3 and 4 (Mosa et al., 2019):

$$Z_{\text{total}} = Z_{MPP} + Z_D \quad (3)$$

$$\alpha = \frac{4\text{Re}\{Z_{\text{Total}}\}}{[1 + \text{Re}\{Z_{\text{Total}}\}]^2 + [\text{imag}\{Z_{\text{Total}}\}]^2} \quad (4)$$

Where η represents the kinematic-viscosity of air, $x = ((d)/(2))\sqrt{(\omega\rho/\eta)}$ with $\omega = 2\pi f$ is the angular frequency, ρ is the ambient air density, c is the speed of the sound, p is perforation ratio, t is the panel thickness, d is the hole diameter and $j = \sqrt{-1}$, and D is the depth of the air cavity between the MPP and the rigid wall.

2.2. Design of Experiment (DoE)

Utilizing the Design of Experiment (DoE) method is needed to characterize an effective range of working conditions in multivariate systems. Determining the relationship between the model input variables (parameters) and the output of that process can be the main target of this method; furthermore, it is to investigate each parameter affecting the response. Here, the DoE tool is used to determine the relationship between the parameters of a single-layer MPP, namely hole sizes, perforation ratio, depths of the back-air cavity, and the panel thickness with the generated response, which is the sound absorption coefficient. Figure 1 shows the DOE progress methodology flowchart to govern the relationship between the output and the MPP parameters.

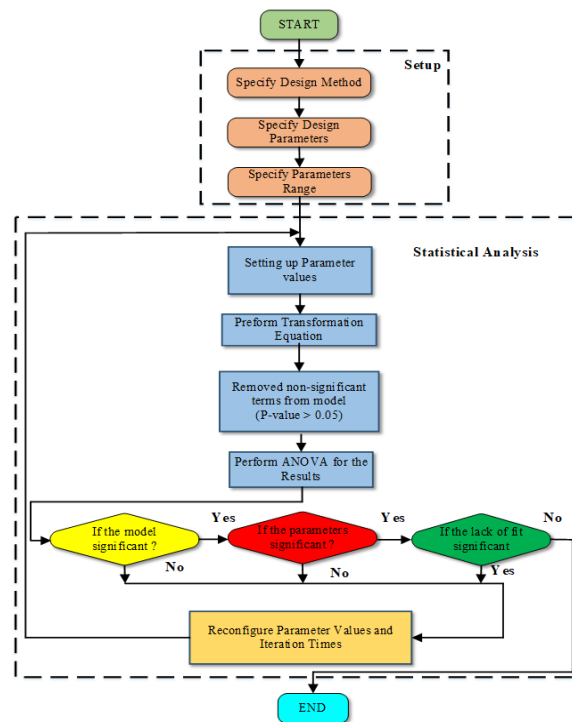


Figure 1 Flowchart of the design experiment methodology

2.3. The utilization of RSM

The term (RSM) can be defined as the “Response Surface Methodology” which is identified as a technique combined of arithmetical and statistical methods. The analyzing process of this method allows for assessing the interactions between the system factors and their effects on response variables (Wang et al., 2017; Deeying et al., 2018). It develops an appropriate approximated relationship between the responses and the input variables. The choice of the varied parameters is according to the required application. Once the parameters are picked, their ranges should be chosen. In this study, the governed relationship is only valid for that corresponding frequency range. Generally, the relationship among the response variable (R) and the predictor variables (v₁, v₂,..., v_i) can be expressed in Equation 5 (Liang et al., 2007):

$$R = g(v_1, v_2, \dots, v_i) + \epsilon \tag{5}$$

Where R is the predicted response, ε is the model error. Usually, low-order polynomial in some regions of the independent variables is used in the RSM, including the first-order model. The response can be expressed in Equation 6:

$$R = \beta_0 + \sum_{i=1}^n \beta_i V_i + \varepsilon \tag{6}$$

A higher degree polynomial function must be utilized, such as the second-order model, if the system behavior cannot be well modeled with a linear equation. The response is expressed in Equation 7:

$$R = \beta_0 + \sum_{i=1}^n \beta_i V_i + \sum_{i=1}^n \beta_{ii} V_i^2 + \sum_{i=1}^n \sum_{i < j} \beta_{ij} V_i V_j + \varepsilon \tag{7}$$

Where β_0 is constant, β_i is the linear effect or can be defined as the slope of the factor V_i . β_{ii} denote the quadratic effect of the factor V_i . β_{ij} is the effect of the interaction between the structure factors V_i and V_j , where ε is the residual term.

The analysis of variance (ANOVA) that supplied the diagnostic inspection tests led to adequacy projected model. As well the optimization predictions can be obtained by using RSM. Consider a simple case where the response variable R is dependent only on two variables V_1 and V_2 , then we can write the second-order model according to equation 7 as the following in Equation 8:

$$R = f(V_1, V_2) + \varepsilon = \beta_0 + \beta_{1 \times 1} + \beta_{2 \times 2} + \varepsilon \tag{8}$$

Usually, the RSM is utilized if the response variable counts on either the mixture of both models or the multiple input variables. In cases like this, the matrix format as $R = V\beta + \varepsilon$ can describe the multiple regression models, where:

$$R = \begin{pmatrix} R_1 \\ R_2 \\ \vdots \\ R_n \end{pmatrix}, X = \begin{pmatrix} 1 & v_{11} & v_{12} & \dots & v_{1p} \\ 1 & v_{21} & v_{22} & \dots & v_{2p} \\ \vdots & \vdots & \vdots & \ddots & \vdots \\ 1 & v_{n1} & v_{n2} & \dots & v_{np} \end{pmatrix}, \beta = \begin{pmatrix} \beta_0 \\ \beta_1 \\ \vdots \\ \beta_p \end{pmatrix} \text{ and } \varepsilon = \begin{pmatrix} \varepsilon_0 \\ \varepsilon_1 \\ \vdots \\ \varepsilon_n \end{pmatrix} \tag{9}$$

The simulated equation 9 produces a multi-dimensional response surface; this response can be utilized to optimize the system according to multiple response variables. Here, the RS model is to be created as a functional relationship among the response of the node of interest and the input structure parameters.

2.4. Central composite design

It is one of the extremely basic RSM augmented that can be symbolized as “CCD” with the center and axial points to fit second-order (quadratic) and cubic models for the response variables. Regularly it has five levels for each input factor. In this work, the CCD is applied with four independent parameters to evaluate their effects on the sound absorption coefficient. The parameters namely frequency range (f), panel hole diameter and perforation ratio (d and p), and the air cavity depth (D). While the thickness of the panel, t remains constant. The various values of each input variable (parameter) are itemized in Table 1. The parameters have been specified according to literature as a simple case chosen for the building acoustics application (Liu et al., 2017; Bucciarelli et al., 2019).

The design implementation includes 24 non-central points and 6 central points. Therefore, a compilation of 300 test points is utilized. The measure of precision is chosen according to center point replication. Then it is followed by entering the model response

data in the design layout; it should choose the response on the corresponding node under analysis.

Transformation of the response is needed as an important component of any data analysis (Wyantuti et al., 2020). An inverse square root transformation has been chosen, and a quadratic model is suggested. The analysis of variance (ANOVA) is obtained through the selected model and the results can be generated.

Table 1 Design level range for the input parameters (independent variables) of the SL-MPP model

Factor	Variable	Units	Lowest value	Highest value
1	d	mm	0.4	0.8
3	p	%	0.5	2.5
5	D	mm	20	60
7	f	Hz	300	900

The response equation in terms of coded parameters was inversely proportional to the four input factors; meanwhile, the response was proportional by actual factors (coded terms). The final equation in terms of basic parameters is given in Equation 10:

$$1/\sqrt{\alpha} = F1 + F2 \times d + F3 \times p + F4 \times D + F5 \times f \quad (10)$$

where parameters coefficients are symbolized by the terms F1 to F5. The predictions around the response for the input factor can be represented by equation 10, where the original units of the elements have to be written in their original units. However, since the parameters coefficients aren't intercepted at the center of the design space and they are scaled to adapt the units of each factor, the calculation of the relative impact of each factor can't be done through this equation.

3. Results and Discussion

3.1. Analysis of the RSM Statistical

As described in the previous, 30 trials using five-level coded independent parameters are taken into consideration for the statistical modelling. Thus, to obtain the regression mathematical model, second-order polynomial functions are used. The general form of the results from the multiple regression analysis of variance (ANOVA) of the response surface is given by selecting the appropriate model either the mean, linear, quadratic, or cubic with interactions that describe the relationship with the response variable. The CCD proposed the experimental combination of the coded levels, and the response are shown in Table 2. The frequency f here represents the input frequency in the range of 300 Hz to 900.

3.2. Analysis of variance (ANOVA)

The investigation of the multiple regression analyzes on the model is important. Here in this work, the process coefficients with model [(Prob > F) < 0.050] are highly significant with neglecting the non-significant terms. The summary statistics depict that the "quadratic model" has the highest determination coefficients, which focus on the model maximizing the "Adjusted R-Squared" and the "Predicted R-Squared". Table 3 shows the final regression analysis of the model. The model show p-value less than (0.0001) with F-value of (52.98), which implies that the model is highly significant. The lack of fit test confirmed the fitness of the model validation with a value of 3.25 (not significance), which confirmed the model appropriateness to predict the variations of the response alpha (which is the sound absorption coefficient) (Bimakr et al., 2019).

Table 2 The CCD for the response predicted values “sound absorption coefficient” for the SL-MPP

Run No.	Factor no.1 d (mm)	Factor no.2 p	Factor no.3 D (mm)	Factor no.4 f (Hz)	Response (Predicted) values Absorption coefficient (α)
1	0.6	0.015	40	900	0.79
2	0.5	0.020	30	450	0.15
3	0.6	0.015	40	600	0.65
4	0.5	0.010	30	750	0.98
5	0.7	0.010	50	450	0.7
6	0.6	0.015	40	300	0.1
.
.
28	0.6	0.025	40	600	0.32
29	0.6	0.015	20	600	0.23
30	0.6	0.015	60	600	0.87

The model accuracy is validated using the “R-Squared (R^2)”, “adjusted R-Squared (Adj R^2)”, “predicted R-Squared (Pred R^2)”, and the value of the coefficient of variance (CV%). The obtained value of the Adj R^2 (0.9517) is closer to the R^2 (0.9700) of the response; also, the Pred- R^2 of (0.8787) is in the acceptable range with the Adj- R^2 . In other words, the contrast is fewer than 0.2 which demonstrates that the generated model can analyze the relationship of the parameters with the response. The CV% is drawn upon to observe the data average value, and it depends on the standard error data between the experimental and predicted values.

Table 3 Assessment of variance ANOVA for Response Surface model

1-Source	2-Sum of Squares	3-df	4-Mean Square	5-F Value	6-p-value Prob > F	
“Model	9.50	11	0.86	52.98	< 0.0001	Significant-
“A-d”	0.20	1	0.20	12.08	0.0027	Significant-
“B-p”	1.10	1	1.10	67.35	< 0.0001	Significant-
“C-D”	1.37	1	1.37	83.72	< 0.0001	Significant-
“D-f”	4.32	1	4.32	264.61	< 0.0001	Significant-
“AD”	0.079	1	0.079	4.83	0.0412	Significant-
“BC”	0.19	1	0.19	11.45	0.0033	Significant-
“BD”	0.41	1	0.41	25.29	< 0.0001	Significant-
“CD”	0.61	1	0.61	37.69	< 0.0001	Significant-
“B2”	0.098	1	0.098	6.01	0.0246	Significant-
“C2”	0.14	1	0.14	8.55	0.0090	Significant-
“D2”	1.15	1	1.15	70.73	< 0.0001	Significant-
Residual	0.29	18	0.016			
Lack of Fit	0.26	13	0.020	3.26	0.0999	not significant-
Pure Error	0.031	5	0.006198			
Std. Dev.	0.13				R-Squared-	0.9700
Mean	1.52				Adj R-Squared-	0.9517
CoV. %	8.43				Pred R-Squared-	0.8787
					Adeq Precision-	25.570

Lower CV% can confirm the reliability of the model, which means a low disparity among the actual and predicted values. Additionally, it approves that the developed model is highly significant for predicting the sound absorption of the MPP model. Then the

ultimate equation in terms of the actual MPP parameters in a frequency range from 300 Hz to 900 Hz is given by the Equation 11:

$$\begin{aligned} 1/\sqrt{\alpha} = & 5.85229 + 3.71379 d + 186.639 p - 0.126313 D - 0.0128599 f - 0.0046795 \\ & d f - 2.16064 p D - 0.214094 p f + 0.000130669 D f + 2367.61 (p)^2 + \\ & 0.000705862 * (D)^2 + 9.02113e-006 (f)^2 \end{aligned} \quad (11)$$

Where, the unit of the hole diameter d , the perforation ratio p , the cavity depth D , and the frequency f are the parameters in MPP, and must have the unit as listed in Table 1. Equation 11 represented the final empirical model that use to predict the sound absorption coefficient, α for the parameters of the given level in the equation.

3.3. Comparison of the empirical model

After the estimated response values have been found, then to verify the empirical model equation 11, 20 combination points of MPP parameters are chosen and utilized in the equation as shown in Table 4.

Table 4 Central Composite Design for the absorption coefficient of Single layer MPP

Run	d (mm)	p (%)	D (mm)	f Hz	Alpha, α (response)		$\frac{\alpha_{Act.}}{\alpha_{Pred.}}$	
					Actual	Predict		
1	0.6	0.015	40	900	0.85	0.82	1.031	
2	0.5	0.02	30	450	0.15	0.36	0.414	
3	0.6	0.015	40	600	0.7	0.80	0.875	
4	0.5	0.01	30	750	0.98	0.98	0.999	
5	0.7	0.01	50	450	0.7	0.68	1.026	
6	0.6	0.015	40	300	0.1	0.34	0.291	
7	0.7	0.02	30	450	0.1	0.32	0.308	
8	0.8	0.015	40	600	0.65	0.70	0.930	
9	0.6	0.015	40	600	0.7	0.80	0.875	
10	0.6	0.005	40	600	0.65	0.94	0.688	
11	0.7	0.02	50	750	0.73	0.92	0.790	
12	0.6	0.015	40	600	0.7	0.80	0.875	
13	0.6	0.015	40	600	0.7	0.80	0.875	
14	0.5	0.01	50	450	0.8	0.87	0.916	
15	0.5	0.02	30	750	0.55	0.75	0.738	
16	0.7	0.01	30	450	0.25	0.47	0.530	
17	0.7	0.02	50	450	0.27	0.50	0.540	
18	0.7	0.01	50	750	0.7	0.84	0.834	
19	0.4	0.015	40	600	0.8	0.94	0.855	
20	0.5	0.01	50	750	0.75	0.87	0.863	
21	0.6	0.015	40	600	0.7	0.80	0.875	
22	0.6	0.015	40	600	0.7	0.80	0.875	
23	0.7	0.02	30	750	0.45	0.72	0.622	
24	0.5	0.02	50	450	0.35	0.60	0.587	
25	0.5	0.01	30	450	0.35	0.56	0.629	
26	0.7	0.01	30	750	0.93	0.94	0.986	
27	0.5	0.02	50	750	0.85	0.96	0.885	
28	0.6	0.025	40	600	0.3	0.52	0.574	
29	0.6	0.015	20	600	0.23	0.50	0.462	
30	0.6	0.015	60	600	0.87	0.95	0.918	
							mean	1.042
							SD	0.151
							CoV%	0.145

The comparison shows a significant convergence between the predicted absorption coefficient values, α , and the actual values. As result, the main value is close to 1, and the coefficient of variation (CoV) approaches 0.145%, which is acceptable (Bimakr et al, 2019).

Figure 2 shows the plot between the predicted data and actual data. According to the results, the distribution of the predicted data to the actual one is very close. This verifies the accuracy of the generated regression in equation 11. The data are distributed normally in a straight line with some fluctuation at some points; thus, the error is insignificant within the range of operating parameters.

The verification of the empirical model is also presented in the form of absorption coefficient via frequency range. Figures 3 (a, b, and c) compare the sound absorption coefficient for SL-MPP between the actual data using the numerical solution and predicted data using the empirical equation 11. Results show a good agreement between the two methods, especially in Figure 3 (a and b) with a slight deviation in (c). Since the model depends on an approximate solution thus, it's normal to get a difference between actual and predicted data. However, both curves have similar behavior, and the slight deviation in frequency, especially in figure (c) is around 10% to 20%, which is in the same range of CoV listed in Table 4 and matches with reference (Bimakr et al., 2019). The developed empirical model can provide accurate results in designing single-layer MPP models.

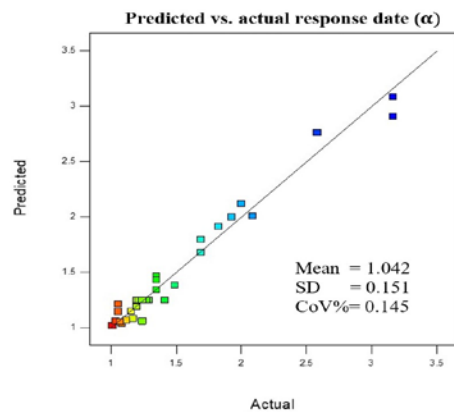


Figure 2 Comparison of absorption coefficient, predicted data via the actual data for SL-MPP

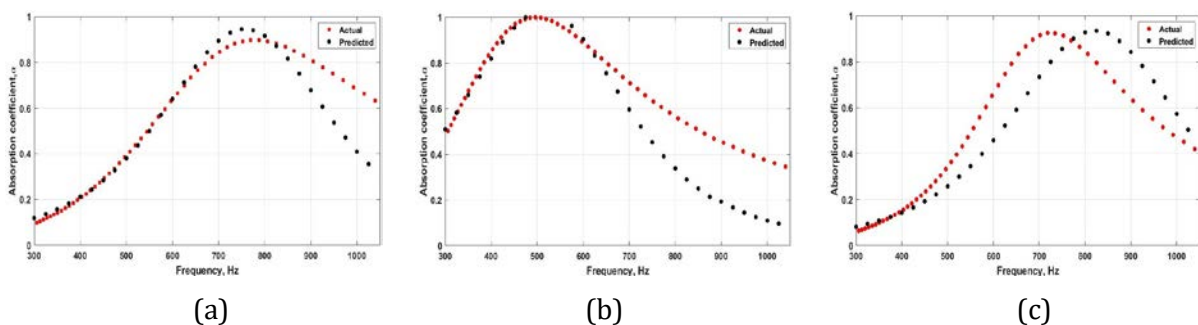


Figure 3 Comparison of sound absorption coefficient between the actual data and predicted data for SL-MPP, (a) d: 6mm, p:0.15%, D:40 mm (b) d: 9mm, p:0.09%, D:60 mm (c) d: 8mm, p:0.1%, D:30 mm

RSM is also utilized to realize the relationship between the tested parameters affecting the response (α). The contour plots are generated to represent the parametric individual combined effects on the absorption coefficient, α for the SL-MPP model. The lower and upper limits of the parameter ranges are determined in this optimization process.

Figure 4 illustrates the contour graphs of the sound absorption coefficient variation against panel hole size and frequency range at constant perforation ratio, $p= 0.02\%$, and for multiple cavity depths of $D = 30$ mm and of $D = 40$ mm. Furthermore, in order to investigate the variation of sound absorption coefficient against panel hole size and perforation ratio, Figure 5 is presented for the frequencies 600 Hz and 900 Hz at a constant cavity depth of $D = 30$ mm. It can be observed from the figure that a decrease in the perforation ratio can

produce a half absorption coefficient $\alpha > 0.5$ for holes diameters range of 0.5 mm to 0.8 mm. however, higher perforation can produce lower values of the absorption coefficient.

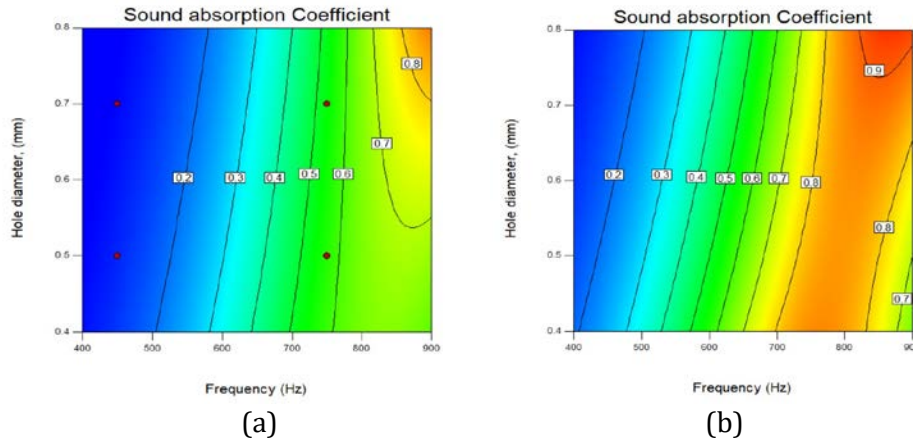


Figure 4 Contour Plots representing sound absorption coefficient variation against panel hole size and frequency range at structure parameters of (a) $D = 30$ mm, (b) $D = 40$ mm

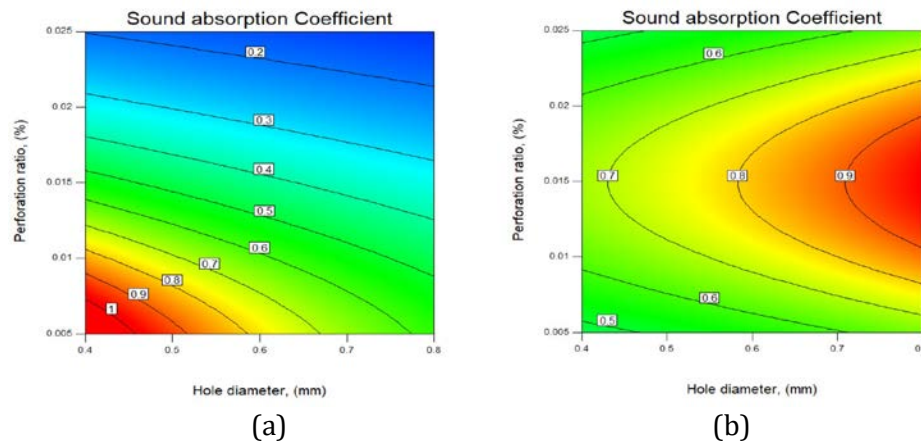


Figure 5 Contour Plots representing sound absorption coefficient variation against panel hole size and perforation ratio at a frequency range of: (a) $freq. = 600$ Hz, (b) $freq. = 900$ Hz

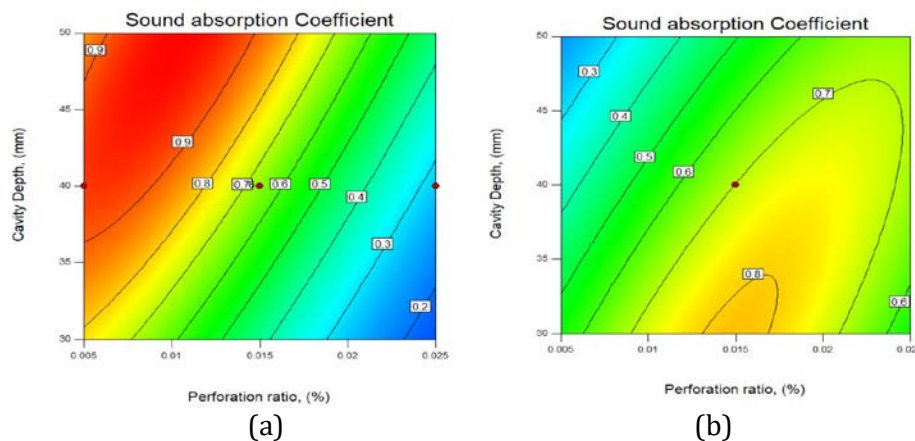


Figure 6 Contour Plots representing sound absorption coefficient variation against panel perforation ratio and cavity depth at a frequency range of: (a) $freq. = 600$ Hz, (b) $freq. = 900$ Hz

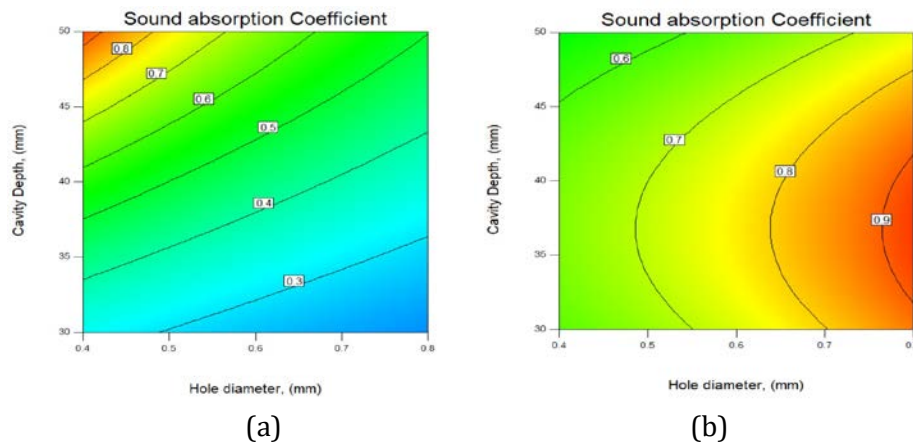


Figure 7 Contour Plots representing sound absorption coefficient variation against panel hole size and cavity depth at a frequency range of: (a) $freq. = 600\text{Hz}$, (b) $freq. = 900\text{Hz}$

In addition, the effect of the cavity depth is an important parameter of absorption response. In order to investigate this effect, Figures 6 and 7 are presented the value of cavity depth against panel perforation ratio and hole size for the frequencies 600 Hz and 900 Hz, at hole size of $d = 0.6\text{ mm}$. It's clear from the figures the cavity depth has a significant impact and can control the absorption bandwidth range. With the results of RSM of equation 7 and the figures below, designers can select the appropriate system structure for the relevant application.

4. Conclusions

The optimized empirical model to calculate the sound absorption coefficient of a single-layer MPP has been presented in this paper. The model was developed using the response surface methodology to generate a second-order polynomial model as a function of MPP parameters, namely the hole diameter, the perforation ratio and the depth of the back air layer. The predicted data is evaluated with the actual data leading to a coefficient of variation of about 0.145%. The predicted model is then verified with the analytical model with good agreement. The proposed model in this paper is however, only valid for the frequency range of 300 – 900 Hz. The same method can be used to generate empirical models of a single layer MPP with a different frequency range of interest. In future work, these empirical models can be utilized as the complete set of mathematical tools to calculate the absorption coefficient of MPP conveniently. The work can also be extended with the more complicated configuration of the MPP structure, such as the double-leaf MPP and the multi-cavity MPP.

Acknowledgements

The authors would like to express their gratitude to Universiti Teknikal Malaysia Melaka (UTeM). Part of this project is supported by the Fundamental Research Grant Scheme from the Ministry of Higher Education Malaysia No. FRGS/1/2016/TK03/FTK-CARE/F00323. The corresponding author would like to express appreciation for the University of Baghdad for its great support.

References

Ahmad, S.H, Salih, R.M., 2020. Acoustic and Thermal Insulation of Nanocomposites for Building Material. *Baghdad Science Journal*, Volume 17 (2), pp. 494–501

- Bimakr, M., Ganjloo, A., Noroozi, A., 2019. Effect of Acoustic Cavitation Phenomenon on Bioactive Compounds Release from *Eryngium Caucasicum* Leaves. *Journal of Food Measurement and Characterization* 13 (3), Volume, pp. 1839–1851
- Boulandet, R., Lissek, H., 2010. Optimization of Electroacoustic Absorbers by Means of Designed Experiments. *Applied Acoustics*, Volume 71 (9), pp. 830–842
- Box, G. E. P., & Wilson, K. B., 1951. On the Experimental Attainment of Optimum Conditions. *Journal of the Royal Statistical Society*, Volume 13(1), pp. 1–38
- Bucciarelli, F., Fierro, G.P.M., Meo, M., 2019. A Multilayer Microperforated Panel Prototype for Broadband Sound Absorption at Low Frequencies. *Applied Acoustics*, Volume 146, pp. 134–144
- Deeying, J., Asawarungsaengkul, K., Chutima, P., 2018. Multi-Objective Optimization on Laser Solder Jet Bonding Process in Head Gimbal Assembly using the Response Surface Methodology. *Optics and Laser Technology*, Volume 98, pp. 158–168
- El-Basheer, T.M., Youssef, R.S., Mohamed, H.K., 2017. NIS Method for Uncertainty Estimation of Airborne Sound Insulation Measurement in Field. *International Journal of Metrology and Quality Engineering*, Volume 8, p. 19
- Harahap, A.F.P., Rahman, A.A., Sadrina, I.N., Gozan, M., 2019. Optimization of Pretreatment Conditions for Microwave-assisted Alkaline Delignification of Empty Fruit Bunch by Response Surface Methodology. *International Journal of Technology*, Volume 10(8), pp. 1479–1487
- Hawashi, M., Aparamarta, H., Widjaja, T., Gunawan, S., 2019. Optimization of Solid State Fermentation Conditions for Cyanide Content Reduction in Cassava Leaves using response surface methodology. *International Journal of Technology*, Volume 10(3), pp. 624–633
- Huang, S., Li, S., Wang, X., Mao, D., 2017. Micro-Perforated Absorbers with Incompletely Partitioned Cavities. *Applied Acoustics*, Volume 126, pp. 114–119
- Hussein, T.M.E.-B., 2020. Calibration and Uncertainty Estimation for the Reference Sound Source in Reverberation Room. *Romanian Journal of Acoustics and Vibration*, Volume 17(2), pp. 118–127
- Kusaka, M., Sakagami, K., Okuzono, T., 2021. A Basic Study on the Absorption Properties and Their Prediction of Heterogeneous Micro-Perforated Panels: A Case Study of Micro-Perforated Panels with Heterogeneous Hole Size and Perforation Ratio. *Acoustics*, Volume 3(3), pp. 473–484
- Liang, X., Lin, Z., Zhu, P., 2007. Acoustic Analysis of Damping Structure with Response Surface Method. *Applied Acoustics*, Volume 68 (9), pp. 1036–1053
- Liu, Z., Zhan, J., Fard, M., and Davy, J.L., 2017. Acoustic Properties of Multilayer Sound Absorbers with a 3D Printed Micro-perforated Panel. *Applied Acoustics*, Volume 121, pp. 25–32
- Maa, D.Y., 1975. Theory and Design of Microperforated Panel Sound-Absorbing Constructions. *Scientia Sinica*, Volume 18(1), pp. 55–71
- Maa, D.Y., 1987. Microperforated-Panel Wideband Absorbers. *Noise Control Engineering Journal*, Volume 29(3), pp. 77–84
- Mosa, A.I., Putra, A., Ramlan, R., Esraa, A.-A., 2018. Micro-Perforated Panel Absorber Arrangement Technique: A Review. *Journal of Advanced Research in Dynamical and Control Systems*, Volume 10(7): 372–381
- Mosa, A.I., Putra, A., Ramlan, R., Prasetyo, I., Esraa, A.-A., 2019. Theoretical Model of Absorption Coefficient of an Inhomogeneous MPP Absorber with Multi-Cavity Depths. *Applied Acoustics*, Volume 146, pp. 409–419

- Niedz, R.P., Evens, T.J., 2016. Design of Experiments (DOE)-History, Concepts, and Relevance to in Vitro Culture. *In Vitro Cellular and Developmental Biology - Plant*, Volume 52 (6), pp. 547–562
- Petrus, H.T.B.M., Olvianas, M., Astuti, W., Nurpratama, M.I., 2021. Valorization of Geothermal Silica and Natural Bentonite through Geopolymerization: A Characterization Study and Response Surface Design. *International Journal of Technology*, Volume 12(1), pp.196–206
- Prasetyo, I., Muqowi, E., Putra, A., Novembrianty, M., Desendra, G., Adhika, D.R., 2020. Modelling Sound Absorption of Tunable Double Layer Woven Fabrics. *Applied Acoustics*, Volume 157, p. 107008
- Prasetyo, I., Sarwono, J., Sihar, I., 2016. Study on Inhomogeneous Perforation Thick Micro-Perforated Panel Sound Absorbers. *Journal of Mechanical Engineering and Sciences (JMES)*, Volume 10(3), pp. 2350–2362
- Prasetyo, I., Sihar, I., Sudarsono, A.S., 2021. Realization of a Thin and Broadband Microperforated Panel (MPP) Sound Absorber. *Applied Acoustics*, Volume 183, p. 108295
- Qian, Y.J., Cui, K., Liu, S.M., Li, Z.B., Kong, D.Y., Sun, S.M., 2014a. Development of Broadband Ultra Micro-Perforated Panels Based on MEMS Technology. *Applied Mechanics and Materials*, Volume 535, pp. 788–795
- Qian, Y.J., Cui, K., Liu, S.M., Li, Z.B., Shao, D.S., Kong, D.Y., Sun, S.M., 2014b. Optimization of Multi-Size Micro-Perforated Panel Absorbers using Multi-Population Genetic Algorithm. *Noise Control Engineering Journal*, Volume 62(1), pp. 37–46
- Saleh, B.J., Saedi, A.Y.F., Al-Aqbi, A.T.Q., Salman, L.A., 2021. Optimum Median Filter Based on Crow Optimisation Algorithm. *Baghdad Science Journal*, Volume 18(3), pp. 614–627
- Tayong, R.B., Jacques, A., Manyo, M., Siryabe, E., Ntamack, G.E., 2018., On the Simultaneous Inversion of Micro-Perforated Panels' Parameters: Application to Single and Double Air-Cavity Backed Systems. *The Journal of the Acoustical Society of America*, Volume 143(4), pp. 2279–2288
- Wahab, H.A., Rus, A.ZM., Abdullah, M.F.L., Abdullah, N.M., 2019. Design of Experiment for Sound Absorption Materials of Microporous Polymer. *In: International Conference on Information Science and Communication Technology (ICISCT) 2019*, pp. 1–7
- Wang, Y., Qin, X., Huang, S., Lu, L., Zhang, Q., Feng, J., 2017. Structural-Borne Acoustics Analysis and Multi-Objective Optimization by using Panel Acoustic Participation and Response Surface Methodology. *Applied Acoustics*, Volume 116, pp. 139–151
- Wyantuti, S., Setyorini, Z., Ishmayana, S., Hartati, Y., Firdaus, M., 2020. Optimisation of Voltammetric Determination of Dysprosium (III) using Plackett-Burman and RSM-CCD Experimental Designs. *Baghdad Science Journal*, Volume 17(4), pp. 1198–1206
- Yang, X., Bai, P., Shen, X., To, S., Chen, L., Zhang, X., Yin, Q., 2019. Optimal Design and Experimental Validation of Sound Absorbing Multilayer Microperforated Panel with Constraint Conditions. *Applied Acoustics*, Volume 146, pp. 334–344
- Yu, X., Cui, F.S., Cheng, L., 2016. On the Acoustic Analysis and Optimization of Ducted Ventilation Systems using a Sub-Structuring Approach. *The Journal of the Acoustical Society of America*, Volume 139 (1), pp. 279–289